Received: 27 October 2017 | Revised: 3 February 2018 | Accepted: 5 February 2018 | Published on: 10 April 2018

DOI: 10.1002/ctpp.201700161

ORIGINAL ARTICLE

Contributions to Plasma Physics

Verification of 5D continuum gyrokinetic code COGENT: Studies of kinetic drift wave instability

Wonjae Lee[1] | M. A. Dorf[2] | M. R. Dorr[2,3] | R. H. Cohen | T. D. Rognlien[2] | J. A. F. Hittinger[2,3] | M. V. Umansky[2] | S. I. Krasheninnikov[1]

[1]Mechanical and Aerospace Engineering, University of California San Diego, San Diego, California, USA
[2]Fusion Energy Science Program, Lawrence Livermore National Laboratory, Livermore, CA, USA
[3]Center for Applied Scientific Computing, Lawrence Livermore National Laboratory, Livermore, CA, USA

***Correspondence**
Wonjae Lee, 9500 Gilman Drive, La Jolla, CA 92093, USA.
Email: wol023@ucsd.edu

Funding Information
This research was supported by the Livermore Graduate Scholar Program. Jacobs School of Engineering, University of California, San Diego, DE-FG02-04ER54739. Lawrence Livermore National Laboratory, DE-AC52-07NA27344.

COGENT (Continuum Gyrokinetic Edge New Technology) is a kinetic plasma simulation code that is being developed by the edge simulation laboratory (ESL) collaboration. The original version of the code has been developed in a 4D phase space (2D configuration space and 2D velocity space) to address kinetic plasma phenomena in a complex magnetic field geometry including the core, magnetic separatrix, and scrape-off layer regions. This work is focused on extending the original 4D phase space to a 5D phase space (3D2V) to address full kinetic turbulences in a tokamak edge region. Here, we report on the current status of 5D COGENT, which presently operates in a shear-less, simple slab geometry. As a verification study, we use the problems of collision-less drift wave instability (universal instability) including its modification in the presence of collisional effects. The simulation model includes the gyrokinetic equations for ion and electron species coupled to the long-wavelength limit of the gyro-Poisson equation. Collisional effects are represented by the Krook collision model. Linear analytical results for the drift mode growth rate and real frequency are recovered, and the non-linear stage is modelled and analysed as well. In addition, extensive 5D runs have been performed to address the effects of the drift wave instability on blob/filamentary structures characteristic of a tokamak edge. A helical-shaped potential perturbation is observed to grow exponentially in time while spinning around the filament axis with electron drift frequency.

KEYWORDS
drift wave, edge, gyrokinetic, kinetic, plasma

1 | INTRODUCTION

The boundary region of a tokamak encompasses the plasma existing between a high-pressure core region and plasma-facing materials. Plasma transport in the boundary region is dominated by instabilities driven by large gradients of the density or temperature. The collisional mean free path in the plasma boundary region can exceed the wavelength of micro-instabilities (e.g., drift wave instabilities), and as a result the plasma species distribution function may deviate from a Maxwellian distribution during instability phenomena. Therefore, a hydrodynamic approach, which assumes a Maxwellian distribution function and is often used to describe axisymmetric edge plasma transport, might not be valid for the edge plasma turbulence. In order to describe weakly collisional boundary plasmas, we consider a gyrokinetic model employed in the Eulerian (continuum) finite-volume code, COGENT.[1–4] The code has been successfully used to model 4D axisymmetric plasma dynamics including pilot studies of the collision-less drift wave instability with a fixed ratio of the parallel and perpendicular wave numbers.[5] Here, we present the initial results from the 5D version of the code, which has recently become operational in a shear-less slab geometry. Our studies include verification[6] of electrostatic simulations of the drift wave instability for various collisionality regimes for the case of a uniform background magnetic field and temperature. In addition, development of the drift wave instability on top of filamentary/blob structures is analysed.

TABLE 1 Simulation parameters

Parameter	Unit	Drift wave simulation	Plasma filament simulation
n_0	m^{-3}	1×10^{20}	1×10^{19}
T_i, T_e	eV	400	400
B	T	3.0	1.5
(L_x, L_y)	cm	(0.8, 0.8)	(4, 4)
L_z	m	$1.7 \sim 20$	1.6
$(N_x, N_y, N_z, N_{v_\parallel}, N_\mu)$	–	(12, 32, 16, 64, 48)	(64, 64, 32, 36, 12)

In the absence of the magnetic field and temperature gradients, the driving mechanisms for the drift wave instability is dissipation, which provides the phase shift between the density and potential perturbations and depends on the collisionality regime of the plasma. If collisions are negligible, the dissipation is provided by the Landau damping, in which case the instability is sometimes called universal. In the opposite limit of strong collisions, the instability is called resistive drift wave instability. An analysis of the electrostatic drift wave instability including the effects of Krook collisions can be found in Ref. [7]. The electromagnetic expansion of this analytical approach can be found in Ref. [8].

The present paper is organized as follows. The governing equations used by the COGENT code are summarized in Section 2. The drift simulation model used for initial verification studies is introduced in Section 3. Finally, the simulation results are presented in Section 4.

2 | THE GYROKINETIC VLASOV–POISSON MODEL FOR COGENT

The COGENT code uses full-f gyrokinetic model written in the conservative form[9]:

$$\frac{\partial(B^*_{\parallel\alpha} f_\alpha)}{\partial t} + \nabla_{\mathbf{R}} \cdot (\dot{\mathbf{R}}_\alpha B^*_{\parallel\alpha} f_\alpha) + \frac{\partial}{\partial v_{\parallel\alpha}}(\dot{v}_{\parallel\alpha} B^*_{\parallel\alpha} f_\alpha) = B^*_{\parallel\alpha} C_\alpha[f_\alpha], \tag{1}$$

where

$$\dot{\mathbf{R}}_\alpha = \dot{\mathbf{R}}_\alpha(\mathbf{R}, v_{\parallel\alpha}, \mu, t) = \frac{v_{\parallel\alpha}}{B^*_{\parallel\alpha}} \mathbf{B}^*_\alpha + \frac{1}{Z_\alpha e B^*_{\parallel\alpha}} \mathbf{b} \times \mathbf{G}_\alpha, \tag{2}$$

$$\dot{v}_{\parallel\alpha} = \dot{v}_{\parallel\alpha}(\mathbf{R}, v_{\parallel\alpha}, \mu, t) = -\frac{1}{m_\alpha B^*_{\parallel\alpha}} \mathbf{B}^*_\alpha \cdot \mathbf{G}_\alpha, \tag{3}$$

and

$$\mathbf{B}^*_\alpha = \mathbf{B}^*_\alpha(\mathbf{R}, v_{\parallel\alpha}) = \mathbf{B} + \frac{m_\alpha v_{\parallel\alpha}}{Z_\alpha e} \nabla_{\mathbf{R}} \times \mathbf{b}, \tag{4}$$

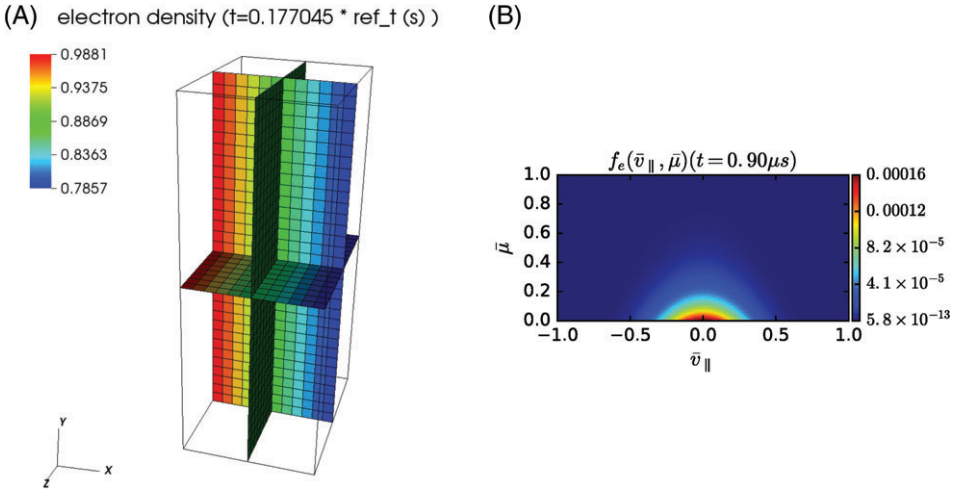

FIGURE 1 Implementation of a 5D phase space in COGENT. (A) Electron density distribution in the 3D configuration space. (B) Electron distribution function in the 2D velocity space. The electron density and potential are normalized to $n_0 = 10^{20}\ m^{-3}$ and $\phi_0 = 400$ V, respectively. Normalization number (ref_t) for the time variable in Frame (A) is 5.11×10^{-6} s

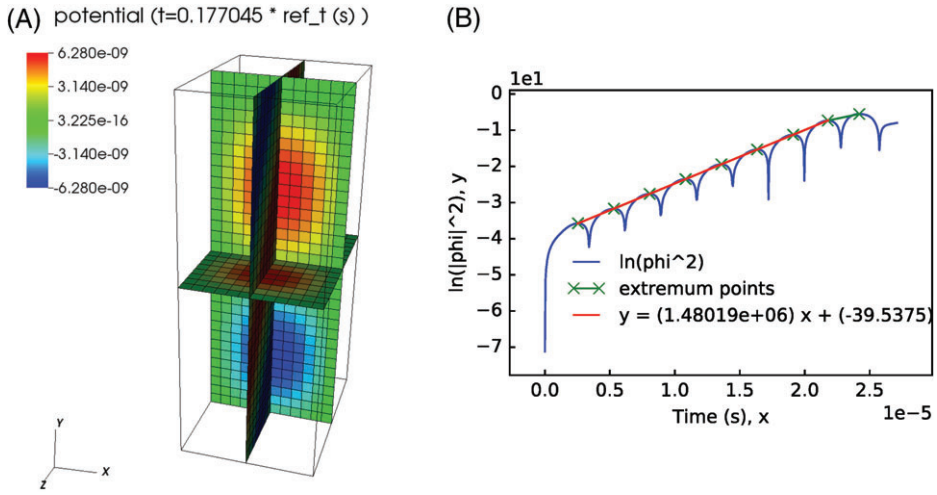

FIGURE 2 (A) 3D electrostatic potential distribution normalized to $\phi_0 = 400$ V. The normalization number (ref_t) for the time variable is 5.11×10^{-6} s. (B) Evaluation of the linear growth rate (red line) from the potential perturbation history (blue curve) obtained in the COGENT simulations of the drift wave instability

$$\mathbf{G}_\alpha = \mathbf{G}_\alpha(\mathbf{R}, v_{\parallel\alpha}, \mu, t) = Z_\alpha e \nabla_{\mathbf{R}} \Phi + \mu \nabla_{\mathbf{R}} B \cdot \tag{5}$$

where $f_\alpha = f_\alpha(\mathbf{R}, v_{\parallel\alpha}, \mu, t)$ is the distribution function for the species $\alpha = \{i, e\}$ in the gyrocenter phase space coordinate $(\mathbf{R}, v_{\parallel\alpha}, \mu)$. $\mathbf{R}$ is the configuration (physical) space, $v_{\parallel\alpha}$ is parallel velocity space component for species α in the direction of magnetic field, and μ is the magnetic moment. The electrostatic potential field Φ is calculated from the long-wavelength limit of the gyro-Poisson equation:

$$\nabla \cdot \left\{ \left[\varepsilon_0 \mathbf{I} + e^2 \sum_i \frac{Z_i \bar{n}_i}{m_i \omega_{ci}^2} (\mathbf{I} - \mathbf{bb}^T) \right] \nabla \Phi \right\} = e \left(n_e - \sum_i Z_i \bar{n}_i \right), \tag{6}$$

where $\bar{n}$ is the ion gyrocenter density, ω_{ci} is ion gyro frequency, and $\mathbf{b}$ is the unit vector in the direction of magnetic field. The present version of 5D COGENT operates in the shear-less slab geometry.

3 | MODELLING DRIFT WAVE INSTABILITY: SIMULATION SET-UP

The 5D version of the COGENT code is verified with simulations of drift wave instability for the case of a uniform magnetic field and temperature background. The simulation parameters are summarized in Table 1. The background electron and ion densities decrease exponentially in the x-direction with gradient scaling length (L_n) in a three-dimensional slab geometry where the magnetic field ($B = 3$ T) is aligned along the z-direction (Figure 1A). The three-dimensional Cartesian computational grid used here has $12 \times 32 \times 16$ cells. The length of the physical domain in the x- and y-direction (L_x, L_y) is 0.8 cm, and the length in the z-direction (L_z) varies from 1.7 to 20 m depending on the simulation case. The electron and ion initial distribution functions are specified by Maxwellian distributions with uniform temperature ($T_i = T_e = 400$ eV) and zero mean velocity. The two-dimensional velocity space consisting of the parallel velocity and the magnetic moment coordinates is divided into 64×48 computation cells, where the computational parallel velocity coordinate $v_{\parallel\alpha}$ is normalized to $\sqrt{T_\alpha / m_\alpha}$. Here, $\alpha = \{e,i\}$ denotes the electron (e) and ion (i) species (Figure 1B).

The initial density profiles of electrons and ions include a small perturbation corresponding to the first harmonic in the periodic (y- and z-) directions. In order to reduce the boundary effect in the x- direction, the initial perturbation is assumed to be negligible at the x-boundaries (Figure 2A). The boundary conditions in the y- and z-direction are taken periodic for the species distribution function and electrostatic potential perturbations. The boundary conditions in the x-direction correspond to the zero Dirichlet boundary condition for the potential, and to the inflow–outflow boundary condition for the species, with $f_\alpha(x_{BC}, y, z, v_\parallel, \mu, t) = f_\alpha(x_{BC}, y, z, v_\parallel, \mu, t = 0)$.

The time integration algorithm utilizes the fourth-order explicit Runge–Kutta (RK4) method, restricted by the Courant constraint. To speed up the simulations, we consider an artificial ion-to-electron mass ratio of 200. The calculated distribution functions of electrons and ions are integrated into the velocity space to form a charge density in each cell of the configuration space. The three-dimensional Poisson solver then calculates the electrostatic potential distribution using this charge distribution. The electrostatic potential is used to calculate the electric field for the next time step.

Here, we consider a simple Krook collision model for electrons, $C_e[f_e] = -\nu_e(f_e - f_{e0})$, where f_{e0} is the initial electron distribution, and ν_e denotes the collision frequency, which is assumed to be spatially constant, for simplicity purposes. Ion

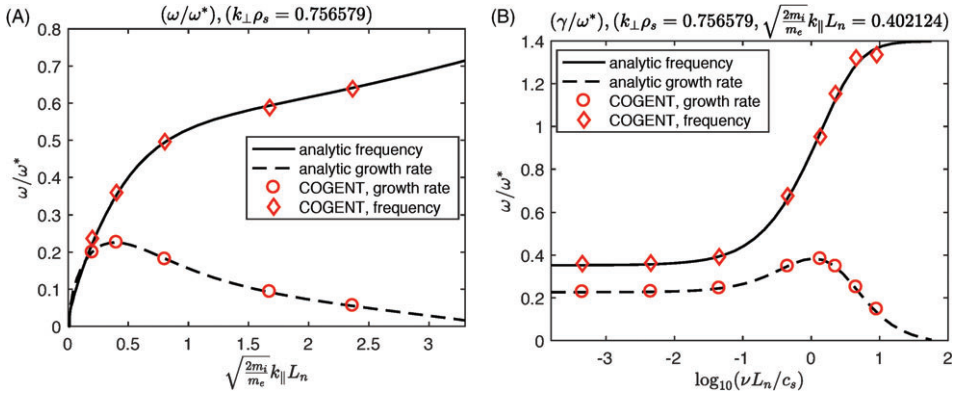

FIGURE 3 COGENT simulation results compared to the analytical predictions in Equation 7: (A) no collisions and (B) including the effects of electron collisions described by the Krook model

collisions are not included. Performing a straightforward linear analysis of Equations 1–6 reported elsewhere,[7,8] we obtain the following drift wave dispersion relation for the case of a uniform background magnetic field and temperature:

$$\frac{T_i}{m_i}\frac{1}{\omega_{ci}^2}\left[-\left(\frac{\omega_{ci}^2}{\omega_{pi}^2}+1\right)k_x^2-\left(\frac{\omega_{ci}^2}{\omega_{pi}^2}+b_z^2\right)k_y^2-\frac{\omega_{ci}^2}{\omega_{pi}^2}k_z^2\right]$$
$$=1+\left[\frac{\hat{\omega}}{\hat{k}_z}+\frac{T_i}{T_e}\frac{\hat{k}_y}{\hat{k}_z}\right]\sqrt{\frac{m_iT_e}{m_eT_i}}Z\left(\frac{\hat{\omega}}{\hat{k}_z}\sqrt{\frac{m_iT_e}{m_eT_i}}\right)+\frac{T_i}{T_e}+\left[\frac{T_i}{T_e}\frac{\hat{\omega}+i\hat{\nu}_e}{\hat{k}_z}-\frac{T_i}{T_e}\frac{\hat{k}_y}{\hat{k}_z}\right]Z\left(\frac{\hat{\omega}+i\hat{\nu}_e}{\hat{k}_z}\right), \tag{7}$$

where Z is the plasma dispersion function, $\hat{\omega}=\omega L_n/c_s$, $\hat{\nu}_e=\nu_e L_n/c_s$, $\hat{k}_y=k_y\rho_s$, $\hat{k}_z=k_z(L_n v_{\mathrm{th},e})/c_s$ and $\rho_s=c_s/\omega_{ci}$, and we have assumed $k_xL_n\gg 1$. We solve this dispersion relation numerically to find the maximum growth rate and the corresponding real frequency for the parameters of COGENT simulations.

4 | RESULT OF NUMERICAL SIMULATIONS

The verification of COGENT code was done by comparing the growth rate and the corresponding real frequency of the drift wave instability extracted from the simulation results with the approximate theoretical predictions for the maximum growth rate and the corresponding real frequency from the wave dispersion relation (Equation 7). In order to obtain the linear drift mode growth rate and frequency from the COGENT simulations, a post-processing of a potential perturbation time history is performed, as shown in Figure 2B. Figure 3A and B illustrate the excellent agreement with the approximate analytical results for the collision-less case and the case with the electron Krook collision model (see Section 3), respectively.

We note that collision-less drift wave is driven unstable by the wave–particle interaction mechanism. Figure 4A and B show the deviation of the electron distribution function from the Maxwellian distribution. Kinetic particles with velocities near the

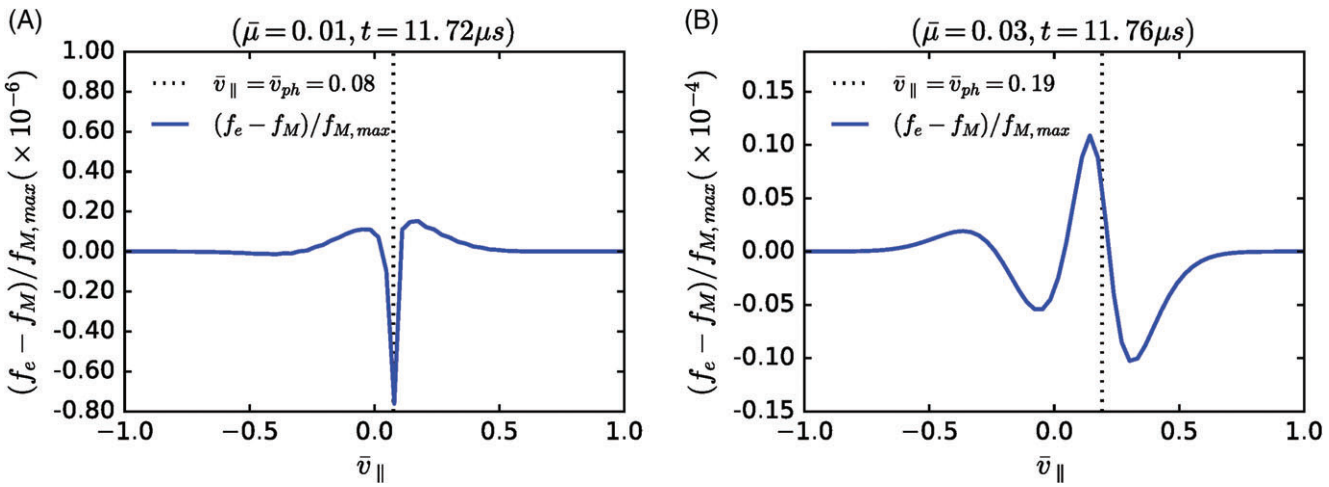

FIGURE 4 Pronounced deviations of the electron distribution function from the Maxwellian background observed for the collision-less case near the drift wave phase velocity due to wave–particle resonance. The normalized drift wave phase velocity (v_{ph}) is illustrated by the dotted line. The results of the simulations in Frames (A) and (B) correspond to low ($\gamma/\omega^*=0.1$) and high ($\gamma/\omega^*=0.23$) values of the growth rate, respectively. $\bar{v}_\parallel$ and $\bar{\mu}$ are the normalized parallel velocity and normalized magnetic moment, respectively

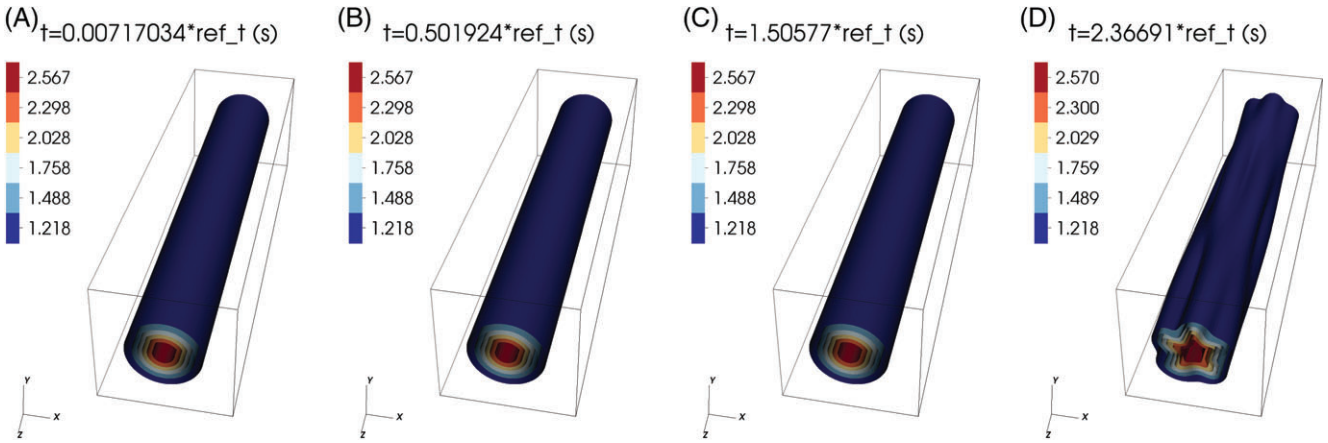

FIGURE 5 Development of the collision-less drift wave instability on a blob-filamentary plasma structure extended along the magnetic field lines. Plotted is the normalized plasma density isosurfaces. The time variable is normalized to the reference time (ref_t = 5.11×10^{-6} s). The filament structure is shown not to scale for visualization purposes

drift wave phase speed experience Landau resonances. The width (Δv) of the perturbation of distribution function is consistent with strength of the instability, $\gamma \sim k_{\|} \Delta v$.

We also investigate the development of the collision-less drift wave instability on an isolated plasma filamentary structure extended along the magnetic field lines (Figure 5). The particle density is set to 1×10^{19} m^{-3}, the species temperature is $T_i = T_e = 400$ eV, and the magnetic field strength is $B = 1.5$ T. The domain size along the magnetic field direction (L_z) is 1.6 m, and the domain extent in the perpendicular directions (L_x, L_y) is 4 cm. The computation domain resolution is given by $(N_x, N_y, N_z, N_{v_{\|}}, N_{\mu}) \leftrightarrow (64, 64, 32, 36, 12)$. See Table 1.

An exponential growth of helix-shaped potential perturbations is observed inside the filament. The perturbations spin around the filament axis with the electron drift frequency. For these simulations, a random-noise perturbation (Figure 6A) is introduced to the filament equilibrium background, and a perturbation mode ($m_\theta = 2$) is observed to be dominant at early stages of the simulations (Figure 6B). However, later in time, a higher order unstable mode ($m_\theta = 3$) takes over (Figure 6C), and its non-linear saturation is shown in Figure 5D.

5 | CONCLUSION

We presented the initial simulations performed with the shearless slab 5D version of the COGENT code. The simulations included the gyrokinetic modelling of the drift wave instability in the presence of electron collisions described by the Krook operator. The linear results of COGENT simulations demonstrated excellent agreement with numerical solutions to a theoretical model. In addition, the 5D code was applied to investigate the effects of collision-less drift wave instability in a

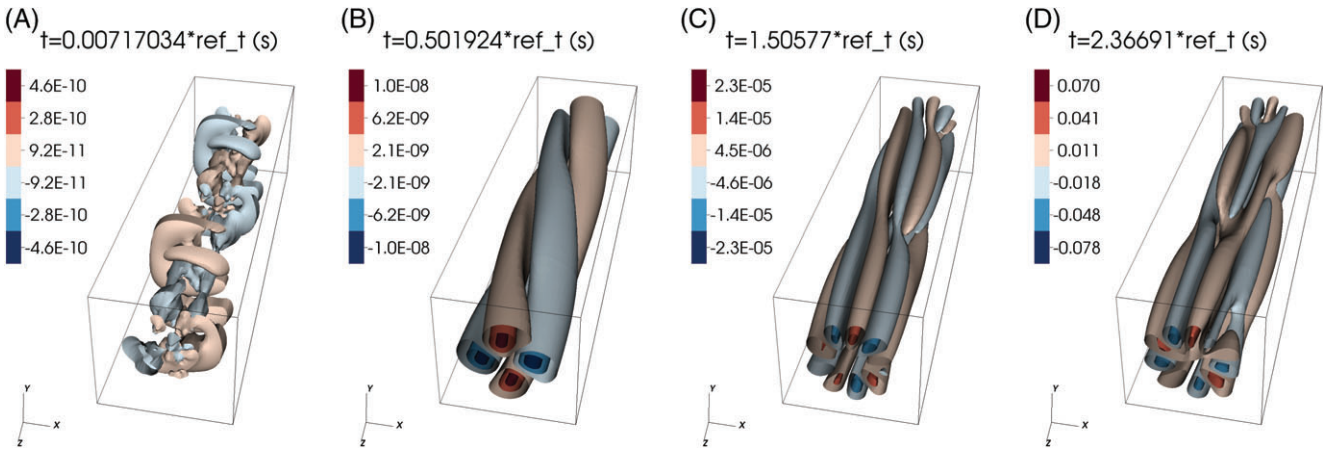

FIGURE 6 Development of helical electrostatic potential perturbations inside the blob-filamentary structure. The helical perturbations rotate around the blob axis with the electron drift speed. The time variable is normalized to the reference time (ref_t = 5.11×10^{-6} s). The filament structure is shown not to scale for visualization purposes

blob-filamentary plasma structure, which is often observed in the boundary region. The linear development and non-linear saturation of noise-seeded helix-shaped perturbations were observed.

ACKNOWLEDGEMENTS

This work was performed for U.S. DOE, at UCSD under Grants DE-FG02-04ER54739 and DE-SC0016548, and at LLNL under contract DE-AC52-07NA27344 and under Livermore Graduate Scholar Program at LLNL. This material is based upon work supported by the U.S. DOE, Office of Science, Fusion Energy Sciences.

REFERENCES

[1] M. A. Dorf, R. H. Cohen, J. C. Compton, M. Dorr, T. D. Rognlien, J. Angus, S. Krasheninnikov, P. Colella, D. Martin, P. McCorquodale, *Contrib. Plasma Physics* **2012**, *52*(5–6), 518.
[2] M. A. Dorf, R. H. Cohen, M. Dorr, J. Hittinger, T. D. Rognlien, *Contrib. Plasma Physics* **2014**, *54*(4–6), 517.
[3] M. A. Dorf, R. H. Cohen, M. Dorr, T. Rognlien, J. Hittinger, J. Compton, P. Colella, D. Martin, P. McCorquodale, *Phys. Plasmas* **2013**, *20*(1), 012513. https://doi.org/10.1063/1.4776712.
[4] M. A. Dorf, M. R. Dorr, J. A. Hittinger, R. H. Cohen, T. D. Rognlien, *Phys. Plasmas* **2016**, *23*(5), 056102. https://doi.org/10.1063/1.4943106.
[5] M. A. Dorf, M. R. Dorr, J. A. Hittinger, W. Lee, D. Ghosh, Conservative high-order finite-volume modeling of drift waves, unpublished.
[6] M. Greenwald, *Phys. Plasmas* **2010**, *17*(5), 058101.
[7] J. R. Angus, S. I. Krasheninnikov, *Phys. Plasmas* **2012**, *19*(5), 052504.
[8] W. Lee, J. R. Angus, S. I. Krasheninnikov, *Phys. Plasmas* **2015**, *22*(7), 072113. https://doi.org/10.1063/1.4927135.
[9] T. S. Hahm, *Phys. Plasmas* **1996**, *3*(12), 4658. https://doi.org/10.1063/1.872034.

How to cite this article: Lee W, Dorf M.A, Dorr M.R, Cohen R.H, Rognlien T.D, Hittinger J.A, Umansky M.V, Krasheninnikov S.I. Verification of 5D continuum gyrokinetic code COGENT: Studies of kinetic drift wave instability, *Contributions to Plasma Physics* 2018;58:445–450. https://doi.org/10.1002/ctpp.201700161.